New spin source to search for scalar-pseudoscalar couplings at short range

G. D. Hammond, A. Pulido Patón,* C. C. Speake,‡ and C. Trenkel†
Gravitation Group, University of Birmingham, Birmingham, B15 2TT, United Kingdom

G. K. Rochester, D. Shaul, and T. J. Sumner
Astrophysics Group, Imperial College London, London, SW7 2AZ, United Kingdom
(Received 15 June 2007; published 19 February 2008)

We describe the design and performance of a new source of polarized spins that can be employed in experiments that search for macroscopic interactions between particles with intrinsic spin. In this article we concentrate on the analysis of the performance of the spin source in generating putative scalar-pseudoscalar forces. We outline two methods of calculating the magnitude of such forces and compare the predictions of the models. We discuss the manufacture of the spin source and the measurements that we have carried out in order to place upper limits on systematic effects that would limit the sensitivity of such searches. We have shown, in a recent article to Physical Review Letters [G. D. Hammond, C. C. Speake, C. Trenkel, and A. Pulido-Patón, Phys. Rev. Lett. 98, 081101 (2007)], that the combination of the spin source together with the torque sensitivity of our torsion balance improves constraints on the coupling strength of macroscopic scalar-pseudoscalar interactions by 10 orders of magnitude at a range of 1 mm. This paper further supports that work and provides a detailed description and characterization of the spin source.

DOI: 10.1103/PhysRevD.77.036005 PACS numbers: 11.30.Er, 12.20.Fv

I. INTRODUCTION

The possibility of there being an interaction directly coupling to the intrinsic spin of elementary particles has been suggested repeatedly within conceptually different theoretical frameworks. For example, a spin-dependent component of the gravitational force has been speculated upon [1]. In particle physics, the most elegant solution to the so-called Strong CP problem invokes a new particle, the axion, which would have spin-dependent couplings [2]. Finally, several extensions beyond the standard model comprise new symmetries, broken at low energies, resulting in a variety of candidates for mediating bosons coupling to spin [3,4].

In general, these mediating particles can have scalar (spin-independent) and pseudoscalar (spin-dependent) couplings, and can therefore lead to three different interactions [5]: (scalar-scalar), (scalar-pseudoscalar) and (pseudoscalar-pseudoscalar). In particular, the interaction potential with mixed couplings can be parametrized as

$$V(r) = g_p g_s \frac{\hbar^2}{8\pi m_{\mathrm{spin}}} \vec{\sigma} \cdot \hat{r}\left(\frac{1}{\lambda r} + \frac{1}{r^2}\right) e^{-r/\lambda} \qquad (1)$$

where g_p denotes the pseudoscalar and g_s the scalar coupling constants, respectively, λ is the range of the new interaction, $\vec{\sigma}$ is the spin of the polarized fermion, and m_{spin} is its mass. In our own experiment we search for couplings to electronic spins, and hence $m_{\mathrm{spin}} = m_e$. One property unique to the mixed interaction is that the $\vec{\sigma} \cdot \hat{r}$ term violates parity and time reversal symmetries on a macroscopic level, which has never been observed in nature. Therefore, in principle, the systematic background due to other known forces should be much reduced.

Theoretical predictions regarding the range and coupling strength of these possible interactions are vague (with the exception, perhaps, of the axion), and therefore any certain knowledge about their parameters results from direct experimental searches. For ranges between 0.1 mm and 1 m, the tightest constraints [6–8] are summarized in Fig. 1. For comparison, the gravitational interaction between an electron and a nucleon, separated by λ, is also shown. It should be noted that a short-range test using a

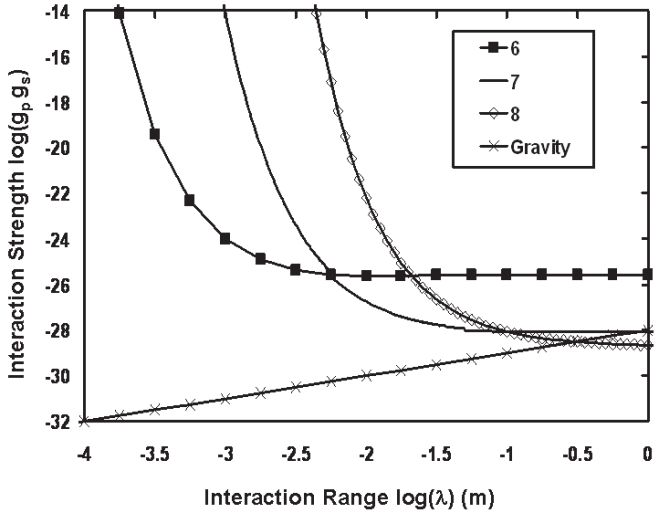

FIG. 1. Current experimental limits on scalar-pseudoscalar couplings as a function of interaction range.

*Purple Mountain Observatory, Chinese Academy of Sciences, Nanjing, 210008, China
†Astrium UK, Gunnels Wood Road, Stevenage, Hertfordshire, SG1 2AS, United Kingdom
‡Corresponding author: c.c.speake@bham.ac.uk

torsion balance with a spin-polarized source mass [9] gave a limit of $g_p g_s < 1.2 \times 10^{-22}$ at a range of $\lambda = 1$ mm. However a full discussion of systematic effects has not, so far, been published for this work. It can be seen that at ranges larger than about 30 cm, new forces of strength comparable with or weaker than gravity have been constrained. At ranges shorter than that, forces many orders of magnitude stronger than gravity may exist.

Most of the experiments searching for a new interaction between spin and matter employ a macroscopic collection of aligned spins, and investigate its interaction with a macroscopic, unpolarized object. The key to a successful experiment lies in maximizing the spin density in the polarized object while at the same time suppressing the magnetic field associated with the spins.

Here we describe and characterize a new macroscopic spin source that has been used to search for an interaction potential of the type given in Eq. (1). The work has already been presented in Ref. [6] and was able to improve limits on the coupling strength of macroscopic scalar-pseudoscalar interactions by 10 orders of magnitude at a range of 1 mm. It is strongly suggested that reading this article will give the reader a better understanding of the current paper in the context of the spin coupling measurement and the method by which systematic effects were handled in the final published result. This article deals in detail with the design and characterization of the spin source used in that work.

In principle, the spin source could also be used to investigate (pseudoscalar-pseudoscalar) couplings, if the second object, the test mass, were also polarized. The novel design of the spin source minimizes magnetic background effects and is optimized for a range of a few millimeters. It is operated in a cryogenic environment, where we can take advantage of superconducting magnetic shielding. The spin source was designed at the University of Birmingham and manufactured at Imperial College, London.

II. SPIN SOURCE DESCRIPTION

A. Design and operating principle

The primary purpose of the spin source is to align a macroscopic quantity of electronic spins. At the same time, the suppression of the magnetic induction field (hereafter referred to as the field) due to these spins at the location of the unpolarized test masses is essential. Our design is based on the principle of magnetic shielding inside a high permeability tube. Figure 2 shows a schematic diagram of one test mass surrounded by one of these tubes. We will refer to these tubes as ''cores'' hereafter. An electromagnet generates an external magnetic field, polarizing the cores such that the region inside is shielded from the external field. The spins inside the core wall generate a magnetic field equal and opposite (to a large degree) to the external field, resulting in the familiar phenomenon of magnetic shielding. Thus, the magnetic field associated with the spins is actually used to minimize the field that is used to align them in the first place. Modulation of the current driving the electromagnet modulates the orientation of the spins. If an interaction potential such as that given in Eq. (1) exists, it will result in a modulated force acting on the test mass, and the resulting motion can be monitored. The residual field at the test mass location is further reduced to negligible levels using superconducting shielding, not shown in the figure. The superconducting shielding arises due to the correlated motion of pairs of electrons with spin-up and spin-down. The net spin of the superconductor is therefore zero and therefore does not behave as a source of a mass-spin coupling force.

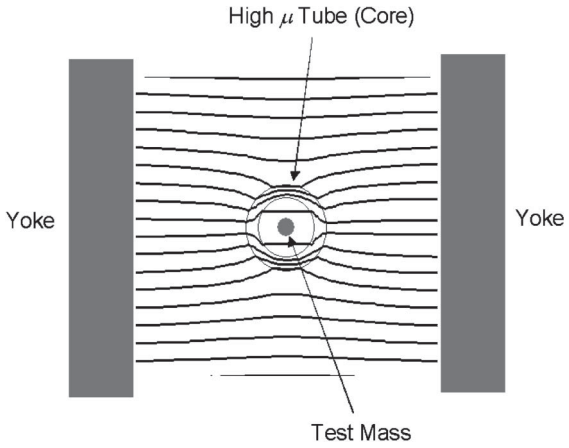

FIG. 2. Interaction region showing a test mass surrounded by a high permeability core, and how external magnetic field lines are ''sucked'' into the core.

It is worth noting that a high permeability of the tubes is important in reducing the residual magnetic fields on the inside, but does not significantly affect the signal strength (provided $\mu \gg 1$). This can be easily seen as follows: the residual H-field inside a cylindrical tube of inner/(outer) radius a/(b) is given by [10]

$$|H_{\rm res}| \approx \frac{4H_0}{\mu}\left[\frac{1}{1 - a^2/b^2}\right] \tag{2}$$

where H_0 is the external field. For the case of a cylinder with small wall thickness, t, compared to its average radius we find that,

$$|H_{\rm res}| \approx \frac{4H_0}{\mu}\left[\frac{b^2}{(b + a)(b - a)}\right] \approx \frac{2b}{\mu t}H_0. \tag{3}$$

Using the expression $H_{\rm res} = H_0 + H_{\rm spins}$ we may write the component of the H-field due to the spins as

$$|H_{\rm spins}| \approx H_0\left(1 - \frac{2b}{\mu t}\right), \tag{4}$$

and we can see that the number of spins that are polarized in a material with $\mu = 100$ is only of the order of 1% less than if the material had, say, $\mu = 10^5$.

B. Experimental configuration and material properties

The overall experimental configuration is shown in Fig. 3(a). The torsion balance that we use to monitor any possible force on the test masses has been previously described in Ref. [11], and the reader is referred to this paper for specific details of the operating principle and performance of the instrument. A photograph of the spin source, with the electromagnet and the three high permeability cores clearly visible, is shown in Fig. 3(b). The electromagnet is made from a toroidal solenoid with three gaps, with each gap accommodating one core and one test mass as described above. We will refer to the three electromagnet sections simply as "yokes." The mean radius of the toroid is approximately 40 mm, and its cross section is approximately 20 mm (width) $\times$ 40 mm (height). High purity soft-iron (99.898% from Blythe Metals Limited) is used as yoke material and has two purposes: First, it reduces the current required in the coil to achieve a given external field at the spin sources and hence the signal strength. Second, the iron serves as a flux guide to minimize flux leakage.

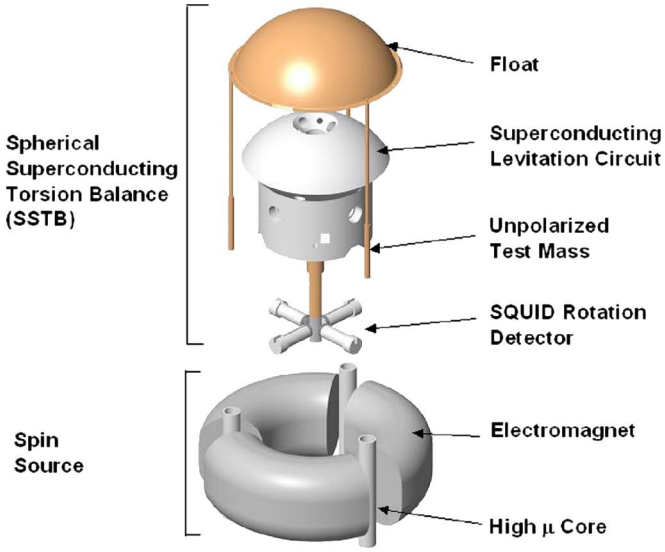

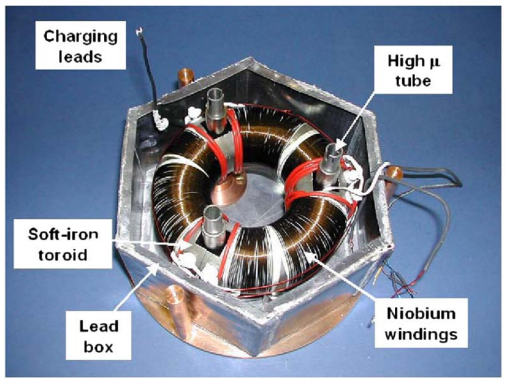

FIG. 3 (color online). (a). Overall experimental configuration showing the Spherical Superconducting Torsion Balance (SSTB) and the spin source. (b) Spin source during assembly, just before the superconducting box is closed. The toroidal electromagnet with windings and high permeability cores are clearly visible.

A reasonably large magnetic permeability, μ_{Toroid}, such that $\mu_{\mathrm{Toroid}} \gg 1$, is required in order to benefit from any field enhancement and confinement. However an extremely large permeability (say $10^4 - 10^5$) would be counterproductive as this reduces the skin depth and hence the frequency necessary for signal modulation. Finally, the material should also exhibit little hysteresis. Significant hysteresis leads to nonlinear behavior and results in heating effects, particularly in a cryogenic environment and given the significant volume (≈ 150 cm^3) of the toroid (see Sec. IV C).

The coil itself and the connections to it are made from niobium (Nb), and a lower limit of 1.25 A has been measured for its critical current. It consists of a total of 722 windings and is connected such that there is no net azimuthal current. The electronic spins in the soft-iron yoke are, of course, also modulated and their contribution to the force that we are looking for needs to be included in the calculations. The gaps are 2.5 cm wide, and therefore the contribution of the yoke spins to the total interaction potential is expected to be negligible at ranges shorter than about 1 cm.

The high permeability cores are made from Mu-Metal supplied by Goodfellow Metals. The outer and inner radii are 6 mm and 4.5 mm, respectively. These dimensions set the fundamental length scale of the experiment. The cores are about 80 mm long in order to make end effects negligible. According to the manufacturer, the material can have a magnetic permeability of up to 2.4×10^5, with a saturation field of 0.77 T (both values are quoted at room temperature). Again low hysteresis is desirable, and we must ensure that the saturation field is not exceeded. The total volume of the three high permeability cores amounts to approximately 6 cm^3. The inside of the cores is lined with a 1 mm thick Nb tube to eliminate any residual fields.

The final component of the spin source, omitted in Fig. 3(a) for clarity, but visible—albeit not fully closed—in Fig. 3(b), is a superconducting box made

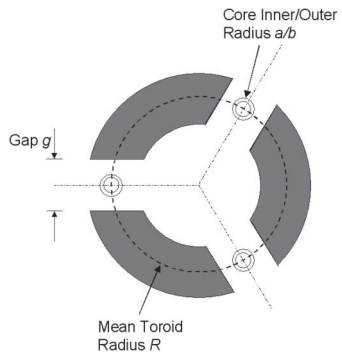

FIG. 4. Schematic cross section through the spin source. The niobium tubes inside the cores are omitted for clarity.

TABLE I. Spin-source parameters.

Parameter	Symbol	Value [m]
Mean toroid radius	R	4.0×10^{-2}
Toroid width	W	2.0×10^{-2}
Toroid height	L	4.0×10^{-2}
Gap	g	2.5×10^{-2}
Core outer radius	b	6.0×10^{-3}

from lead (Pb) foil for the purposes of magnetic shielding. The leads supplying the polarizing current are fed into the box via a long (approximately 50 cm) superconducting Pb tube. Figure 4 shows a schematic cross section of the spin source, showing the toroidal iron yokes as well as the cores. Also indicated are some relevant physical parameters, which will be referred to repeatedly in this document. The values of these parameters are given in Table I.

III. SIGNAL STRENGTH CALCULATION

A new interaction with mixed couplings would exert a force on any test mass placed inside the spin-source cores, and hence result in a torque on our torsion balance that can be monitored. It is clearly necessary to convert the measured torque (or a limit on it if none is observed) into limits on the product of the coupling constants, $g_p g_s$, as a function of range, λ. The interaction potential given in Eq. (1) therefore needs to be integrated over test masses and spin source, differentiated to obtain a force, and then multiplied by the effective armlength of our torsion balance.

The potential, Φ, between a single nucleon and the spin source can be found by integration of Eq. (1) over the volume of the latter. This volume integral can be transformed into a surface integral as follows [12]: with $\vec{\rho}_s$ denoting the local spin density, and defining

$$\phi(r) = -g_p g_s \frac{\hbar^2}{8\pi m_e}\left(\frac{e^{-r/\lambda}}{r}\right) \tag{5}$$

we can write

$$\begin{aligned}\Phi &= \int \vec{\rho}_s \cdot \vec{\nabla}\phi d^3 r \\ &= \int \vec{\nabla}\cdot(\vec{\rho}_s\phi)d^3 r - \int \phi(\vec{\nabla}\cdot\vec{\rho}_s)d^3 r. \end{aligned} \tag{6}$$

The second term on the right-hand side is zero (no divergence inside a homogeneous source) and the first one is equal to a surface integral:

$$\Phi = \int \phi \vec{\rho}_0 \cdot d\vec{S}. \tag{7}$$

As can be seen, a spin source without a leakage field (with all spins tangential to the surface) does not produce a mass-spin coupling interaction potential. In our geometry, this leakage occurs at the *outer* surface of the high permeability tubes (and at the yoke faces). The minimum characteristic separation between test mass and spin signal is therefore given by the outer radius of these tubes.

We have developed two largely independent mathematical models to evaluate the putative signal from new spin sources. We will briefly describe each method in turn, discuss the effect of the various approximations, and finally compare the results.

It is worth noting that both methods require the input of some experimental quantities, in particular, material properties, in order to predict the signal strength. Experiments carried out to measure these quantities are described in Sec. IV.

A. Discrete element method

The first method uses discrete element techniques developed to solve general magnetostatic problems [13,14]. The geometry that was considered is shown in Fig. 5(a): the toroid has a single gap containing a high permeability core. The following further simplifications were made: The normal components of the magnetic field at the surfaces of interest, B_n, were found assuming a 2-D model, i.e. where the dimensions perpendicular to the page in Fig. 5 are assumed to be infinite. The integration of the surface magnetization weighted by the Yukawa potential was evaluated with the full 3-D geometry. The surface spin density is given in terms of B_n as

$$\rho_s = \left(\frac{\mu - 1}{\mu}\right)\frac{B_n}{\mu_0 \mu_B} \tag{8}$$

where μ is the permeability of the material and μ_B the Bohr magneton. The toroidal geometry of the yoke excludes the use of a scalar magnetic potential which in turn implies that, in order to solve for the magnetic flux density, the magnetization of the iron toroid can be taken to be equivalent to a distribution of currents flowing in their surfaces. In our model, we subdivide the surfaces into N discrete bands, and each band is assumed to carry a constant current density. The magnetization of the spin source can be modeled either as surface currents or surface pole densities. We chose the latter for simplicity. The total magnetic field at each surface current or element of surface magnetization will be the superposition of contributions generated by the element itself, and from the fields generated by the other $N - 1$ elements, and from the external current driven through the solenoid. At each surface element on the yokes, the following boundary condition on the tangential field needs to be met:

$$\frac{B_{\text{tangential, outside}}}{\mu_{\text{outside}}} = \frac{B_{\text{tangential, inside}}}{\mu_{\text{inside}}}. \tag{9}$$

The corresponding boundary condition at the elements of surface magnetization on the cores is

$$\mu_{\text{outside}} H_{\text{normal, outside}} = \mu_{\text{inside}} H_{\text{normal, inside}}. \tag{10}$$

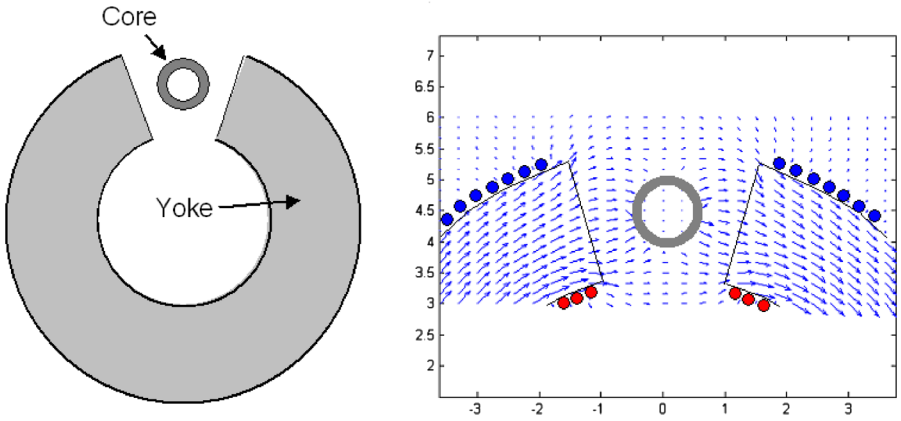

FIG. 5 (color online). (a). Geometry of the numerical model. A toroid with one gap and one core is modeled in 2-D. (b) Magnetic field plot generated using the numerical model

N such conditions result in a system of N linear equations, which is solved by matrix inversion to obtain the N unknown surface currents and pole densities. Once these are found, the normal B-field can be calculated everywhere.

Once the magnetostatic problem is solved, the Yukawa potential given in Eq. (1) is computed, again numerically, through integration of the surface magnetization. Because Eq. (7) evaluates the potential interaction due to a single nucleon, we need to multiply the result by the number of nucleons in a single test mass (i.e. $m_{\text{test-mass}}/m_{\text{proton}}$). Other correction factors to be applied to the result are discussed in Sec. III C.

B. Analytical method

The second method evaluates the Yukawa potential given in Eq. (1) by considering the simplified geometry shown in Fig. 6. A single core and test mass is considered, surrounded by two yoke faces. The core is assumed to be exposed to a uniform external field provided by the electromagnet.

A simple way to estimate this external field is to apply Ampere's law to the toroid with three gaps, ignoring the presence of the cores (this approximation is discussed further in Sec. III C). If N_T denotes the number of turns, g the size of the gap, R the mean radius of the solenoid, and i the current through the solenoid, then the field is given by

$$B_0 = \mu_0 N_T i \left(\frac{2\pi R - 3g}{\mu_{\text{Toroid}}} + 3g\right)^{-1} \approx \frac{\mu_0 N_T i}{3g} \qquad (11)$$

where the second equality applies provided $\mu_{\text{Toroid}} \gg 1$.

The magnetostatic problem of an infinitely long high permeability tube immersed in a uniform field, B_0, with a superconducting tube inside, can be solved in a straightforward manner, and is used to find the radial (normal) component of the spin density $\vec{\rho}_s$ at the outer surface of the tube. This radial component is given by [10]

$$\rho_s(r = b, \varphi) = \left[\frac{2B_0(\mu_{\text{core}} - 1)}{\mu_0 \mu_B}\right] \times \left[\frac{a^2 - b^2}{(\mu_{\text{core}} - 1)a^2 - (\mu_{\text{core}} + 1)b^2} \cos\varphi\right] \qquad (12)$$

in a cylindrical coordinate system (r, φ, z) with the origin on the symmetry axis. The interaction potential is found by using the density defined in Eq. (12) and integrating over the outer core surface. For a single unpolarized test particle located at the origin of the coordinate system (r, $z = 0$), the integration over the angle can be solved analytically. The force (obtained through differentiation of the potential) on this single particle, due to a high permeability tube of length L, is found to be

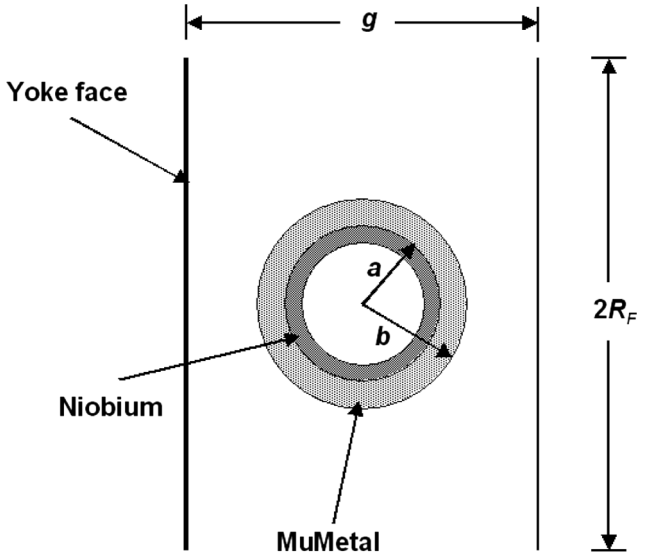

FIG. 6. Geometry of the analytical model. A high permeability core is lined on the inside with niobium and surrounded by two yoke faces. The parameters used in the model are as indicated.

$$F_{\text{Core}} = g_p g_s \frac{\hbar^2}{8\pi m_e}\left[\frac{2B_0(\mu_{\text{core}}-1)}{\mu_0\mu_B}\right] \times\left[\frac{a^2-b^2}{(\mu_{\text{core}}-1)a^2-(\mu_{\text{core}}+1)b^2}\right] \times\int_{-L/2}^{L/2}\left(\frac{1}{(b^2+z^2)^{3/2}} + \frac{1}{\lambda(b^2+z^2)}\right)e^{-(b^2+z^2)^{1/2}/\lambda}dz. \quad (13)$$

The remaining integral in z is solved numerically. It is interesting to note that, in the limit of an infinitely long tube ($L \rightarrow \infty$), a closed expression can be found for the radial force on a point mass, including off-axis points. The radial force on a point at coordinates (r, φ) is

$$F_r(r,\varphi) = g_p g_s \frac{\hbar^2}{m_e}\left[\frac{B_0(\mu_{\text{core}}-1)}{\mu_0\mu_B}\right] \times\left[\frac{a^2-b^2}{(\mu_{\text{core}}-1)a^2-(\mu_{\text{core}}+1)b^2}\right]b\cos\varphi \times\left\{\frac{1}{\lambda}I_0\left(\frac{r}{\lambda}\right)K_1\left(\frac{b}{\lambda}\right)-\frac{1}{r}I_1\left(\frac{r}{\lambda}\right)K_1\left(\frac{b}{\lambda}\right)\right\} \quad (14)$$

where I_0, I_1, and K_1 are modified Bessel functions.

The contribution from the toroidal yoke faces is estimated by assuming a uniform magnetization across these faces, with a normal spin density given by Eq. (8), using the magnetic field given in Eq. (11). The faces were approximated by circles of radius R_F, located a distance $g/2$ away from the origin. The radius R_F was chosen such that the surface area of the circle was equal to that of the actual faces.

The contribution to the total mass-spin force on a nucleon at the origin, due to the magnetization of the yokes, is given by

$$F_{\text{Faces}} = g_p g_s \frac{\hbar^2}{2m_e}\frac{(\mu_{\text{Toroid}}-1)B_0}{\mu_{\text{Toroid}}\mu_0\mu_B} \times\left[\frac{g/2}{\sqrt{(g/2)^2+R_F^2}}e^{-\sqrt{(g/2)^2+R_F^2}/\lambda}-e^{-(g/2)/\lambda}\right], \quad (15)$$

and the total torque on our torsion balance is given by

$$\Gamma_{\text{mass-spin}} = 3\times\frac{m_{\text{test-mass}}}{m_{\text{proton}}}\times(F_{\text{Core}}+F_{\text{Faces}})\times R_{Tb} \quad (16)$$

where the factor 3 reflects the fact that we have 3 test masses, and R_{Tb} is the moment armlength of test masses (approximately 42 mm). $m_{\text{test-mass}}/m_{\text{proton}}$ is, as above, the number of nucleons in one test mass.

C. Approximations and correction factors

Both methods presented above make a number of simplifying assumptions. We need to estimate the effect that these assumptions or approximations have and apply appropriate correction factors to the predicted signal strength.

1. Numerical method

The numerical method described above is a 2-D model which considers one gap in the toroid, one core inside the gap, and computes the total force on just one test mass. The prediction for the magnetic field at the location of the Hall probe, which is attached onto the surface of one of the toroidal yoke faces as shown in Fig. 7, is approximately 5.3×10^{-2}T. Taking into account the finite magnetic permeability of the iron yoke, and the size of the gap (ignoring the presence of the cores), the prediction for the real spin source comprising a toroid with three gaps and cores becomes 2.0×10^{-2}T. The measured value is approximately 2.2×10^{-2}T. It is believed that this 12% discrepancy is due to the effective gap being smaller because of the presence of the cores. No attempt has been made at investigating this further. Because the mass-spin coupling is directly proportional to the magnetic field in the system, we simply apply a positive correction of 12% to the signal calculated using the numerical method. A second approximation results from the fact that the magnetization, and also the spin density, is modeled by piecewise constant surface charges and currents. To test this approximation we observe the convergence as function of element size and test simple, known geometries. We estimate the correction to be -5%. Furthermore, the numerical model uses a 2-D simulation of the magnetic field in which the dimensions in z are assumed to be infinite. By modeling a ''large toroid'' with the thickness equal to the height we observed the field reduction at the radial edges in 2-D and took the average. The correction was -5%. Finally, the faces of the yoke lie along radial lines and this results in an increasing gap with

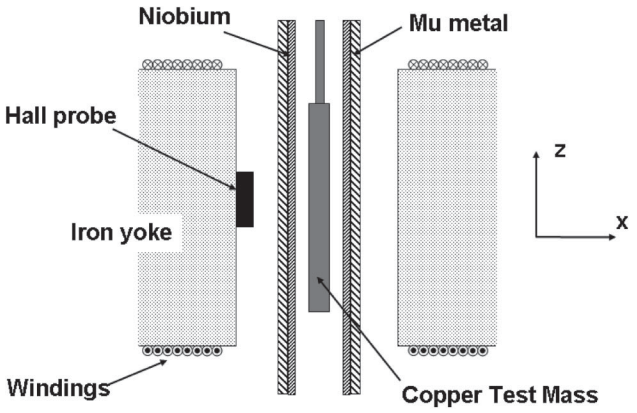

FIG. 7. Schematic side view of a copper test mass inside a core, together with the iron yokes. The Hall probe, used to monitor the magnetic field, is also shown.

increasing radius [compare Figs. 4 and 5(a)]. Comparing the average field across the faces to the field at the midpoint resulted in a correction of -2%.

When the corrections listed above are combined we find that the net effect on the spin signal is negligible.

2. Analytical method

When it comes to assessing how realistic are the approximations made by this method, probably the main difficulty lies in the assumption of an "external" field, B_0, to which the cores are exposed and which also provides the yoke faces with a uniform surface magnetization. In the real geometry, the toroidal gaps are only just over two core diameters wide, and the distance between the cores and the yoke faces is therefore only about one core radius. We expect the field in the gaps to be affected by the presence of the cores themselves (rather than being an external field); this will result in the magnetization across the yoke faces being increased and far from uniform. In order to find the appropriate fields, we have relied on the numerical method, and rescaled the results according to the Hall probe measurements. To some extent, unfortunately, this reduces the independence of the two methods, at least in terms of solving the magnetostatic problem. In this way, the average surface magnetization of the yokes, $B_{0,\text{yokes}}$, has been found to be approximately 1.5×10^{-2} T, i.e. about 25% larger than the 1.2×10^{-2} T from the simple estimate of Eq. (11). This can be understood because the cores are expected to reduce the effective gap. This field will be used to evaluate the yoke contribution in Eq. (15). The problem of the core polarization, and what field to use for it, is less straightforward. We need to find the extent to which the field inside the gap can be approximated by that around a high permeability core exposed to a perfectly uniform field of infinite extent. We have performed numerical simulations that certainly confirm that the field seen by the high permeability core is affected by the presence of the yokes. For a given field measured at the location of the Hall probe, the field just outside the yoke face is about 13% larger than would be expected in the absence of the yokes. It is therefore also to be expected that the measured Hall probe field, even though it is further away, contains *some* contribution from the yokes themselves. A second approximation is that the core polarization is calculated in 2-D assuming a uniform external magnetic field. We have used the numerical method to estimate the field reduction towards edges and then take the average value. This results in a correction of -10%. Furthermore, the polarizing field is assumed to be uniform across the surface of the yoke faces. By comparing the average field across the faces to the field at the midpoint (using numerical method) we estimate a correction of -2%. Finally, the contribution from the yoke is calculated by assuming a circular cross section face with an area identical to the real face. A worst case estimate can be made by using a circular face which has a diameter equal to the yoke height. This results in a correction of $+22\%$ at long ranges only (at ranges shorter than about 1 cm the contribution of the yoke faces is negligible).

The net corrections applied to the analytical results are substantial: the core signal is decreased by approximately 20%, whereas the yoke face signal—which, in terms of mass-spin coupling strength, subtracts from the core contribution—is increased by approximately 20%.

D. Comparison of results

We find that when the correction factors summarized in the previous sections are included there is good agreement between the two calculation methods. The two methods differ by up to 40% at short ranges (smaller than 1 mm, say) and up to 10% at longer ranges. At short ranges the analytical method predicts more strict limits while at long ranges it predicts slightly less strict limits. Given the difficulties in estimating the appropriate fields to be used in the analytical method, and the fact that these estimates ultimately relied on some numerical results as well, we prefer to quote the results from the numerical method. This also provides us with the most conservative constraints at short ranges.

E. Spin density and optimization

In order to compare our spin source with those employed in other experiments, the density of aligned spins is a useful figure of merit. For an external current of 1 A, and the dimensions of the cores mentioned above, we obtain a net alignment of about 10^{22} spins per core. This corresponds to an average spin density of about $5 \times 10^{27}/\text{m}^3$. Internally compensated masses made from Dy_6Fe_{23} achieve spin densities of $2 \times 10^{28}/\text{m}^3$ [7,15], while objects employing macroscopic compensation have spin densities of about $3 \times 10^{27}/\text{m}^3$ [16,17]. It can thus be seen that the spin density of our spin source is comparable with that of other experiments. At least in principle, this density could be increased further by simply increasing the driving current. The largest field generated inside the cores at present is estimated to be about 0.11 T, and this is still much smaller than the saturation field of 0.77 T (see above). In practice, however, significant modifications to our current experimental setup would be required to make full use of such saturation fields. One advantage of our spin source, compared with those mentioned above, is that its polarization can be reversed electronically, rather than by physical rotation of the polarized object.

IV. EXPERIMENTAL SPIN-SOURCE CHARACTERIZATION

In this section we investigate whether the real physical spin source that has been manufactured is capable of realizing its potential as discussed above. Two aspects need to be verified: that the signal strength estimate above is in fact

generated, and that systematic magnetic and thermal background effects are sufficiently small, so that the high sensitivity of the torsion balance can be fully exploited.

A. Signal strength

1. Signal characterization and hysteretic effects

Our experiment consists of energizing the spin-source electromagnet using an alternating current of a single frequency. Any interaction of the form given in Eq. (1) would result in a measured torque occurring at the same frequency and with a possible well-defined phase (see below) relative to the driving current.

Hysteretic effects in the toroidal yoke and/or the cores can lead to the spins behaving differently to the driving current. For example, there may be a significant phase lag between driving current (effectively H) and spin orientation (effectively B). Furthermore, if either the toroidal yoke or the spin-source cores are driven close to their saturation field, the response of the spins will be distorted, resulting in higher frequency components. In order to minimize hysteretic effects, the high μ cores were thermally annealed prior to our experiments, according to the prescription provided by the manufacturer. However, we have not found a suitable way (thermally or magnetically) to anneal the much larger toroidal yokes.

In order to monitor as directly as possible the behavior of the spins inside the cores, we use a cryogenic Hall probe (Lakeshore, model HGCT). This Hall probe is placed in one of the gaps, directly adjacent to one of the cores (see Fig. 7). Because of its close proximity to the core, the measured magnetic field is expected to be a combination of that generated by the yokes (about 55% according to our calculations based on the analytical method as described above), and that generated by the spins in the cores (about 45% according to those same calculations). Currents of $i_{\mathrm{peak}} \approx 0.5$ A and 1 A were driven through the toroidal coil, modulated at a frequency of 12.5 mHz (period 80 s). This is a typical frequency that we use in our experiments. We have measured the modulating current (corresponding to H) and the output from the Hall probe (corresponding to B), just outside the material, as a function of time. Figure 8(a) shows the resulting hysteresis curve, and Fig. 8(b) shows the amplitude spectral density of the Hall probe output. Several observations can be made:

(i) Signal magnitude: The calibration of our Hall probe, provided by Lakeshore, quotes a transfer function of 8.4 mV/T. For a current of 1 A, the measured voltage is equivalent to a peak magnetic field of approximately 2.2×10^{-2} T just outside the cores. A naive estimate based on the analytical method (see Sec. III C) would result in a value of about $B \approx 2.1 \times 10^{-2}$ T, whereas the numerical method predicts $B \approx 2.0 \times 10^{-2}$ T (no correction factors applied in either case). This measurement alone is evidence for both $\mu_{\mathrm{Cores}} \gg 1$ and $\mu_{\mathrm{Toroid}} \gg 1$, and evidence for the spins in the core being modulated as expected.

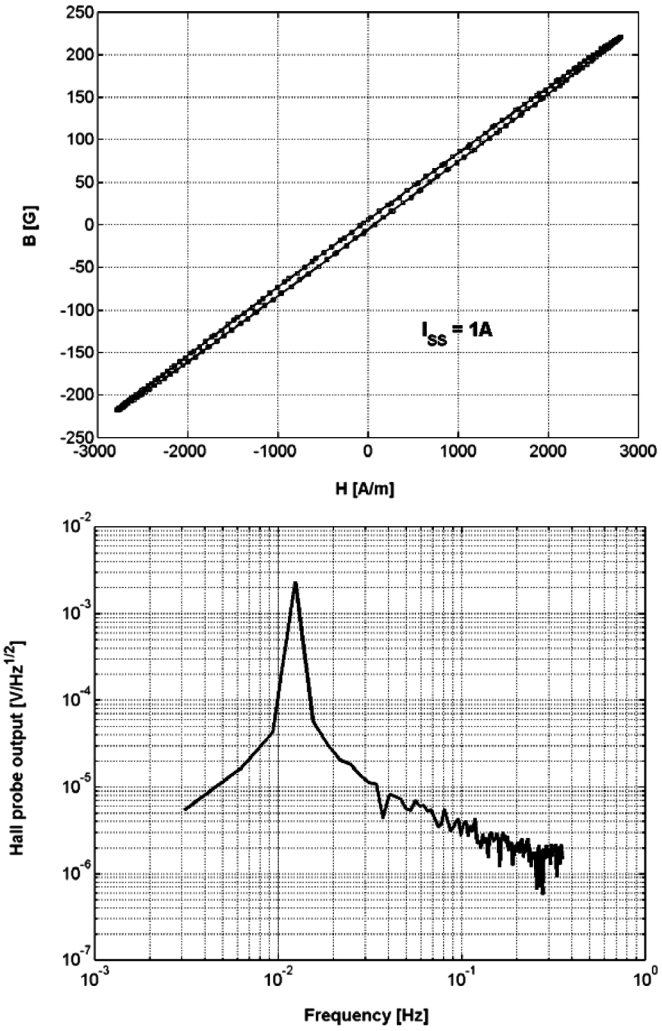

FIG. 8. (a). Hysteresis plot for a spin-source current of 1 A. (b) Frequency spectrum of the Hall probe output for 1 A spin-source current

(ii) There is a phase lag of about 2° between the driving current (the H-field) and the magnetic field. A nonzero phase lag implies energy dissipation in the material, given by $Q = \int H dB$ per unit volume and per period. Assuming that the dominant dissipation takes place in the toroidal yokes, rather than in the cores (simply because of the much larger volume), we estimate a dissipative rms power of about 10 μW. It is also worth noting that this heating is modulated at twice the signal frequency (see Sec. IV C. for more details on heating effects).

(iii) Distortion and nonlinearity: The Hall probe output shows perhaps a small feature ($< 1\%$ of the fundamental peak) at the first odd harmonic, but no other sign of distortion. We also find no significant ($< 0.1\%$) deviation from linearity between currents of 0.5 A and 1.0 A, at the fundamental signal frequency.

This confirms that, as was expected from the calculations, neither the toroid nor the cores are driven into saturation for these currents.

(iv) In the absence of any driving current, we have used the Hall probe to set upper limits on any remnant field, *in situ* and at 4.2 K, of about 10^{-4} T. At room temperature, we have used a more sensitive fluxgate magnetometer to search for offset fields due to the toroid alone, and found nonzero fields of up to 10^{-5} T. Equally we have looked for remnant fields around the cores separately, and found nonzero fields of up to 5×10^{-6} T. All these measurements again point to a very small residual magnetization of the magnetic materials used in the experiment.

The output from the Hall probe is not very sensitive to the permeabilities of the toroid and the cores, and only confirms that $\mu_{\mathrm{Cores}} \gg 1$ and $\mu_{\mathrm{Toroid}} \gg 1$. In order to get a more precise estimate of the permeabilities, we have carried out some dedicated measurements.

2. Permeability of the mu-metal cores

In order to measure the permeability of the cores we have carried out a direct attenuation experiment, comparing the magnetic field outside the cores with the field inside (the niobium shield was removed for this purpose). As mentioned above, if we are polarizing the spins this should lead to magnetic shielding on the inside. We have indeed found an attenuation factor of about 30, and from this we calculate the permeability of the high μ cores at low temperatures to be $\mu_{\mathrm{Cores}}(4.2\ \mathrm{K}) \geq 260$. This value is much lower than the one quoted by the manufacturer at room temperature. We can think of two reasons for this: First, the permeability of the core material is expected to decrease at low temperatures. Second, we have ignored end effects and possible leakage fields, which results in an underestimate of the real permeability. Because the value that we have measured is sufficient to ensure a signal strength within about 1% of the infinite permeability case, we have not pursued this question any further.

3. Permeability of the toroid

In order to estimate the permeability of the toroidal yokes we have carried out inductance measurements at frequencies between 0.25 Hz and 20 Hz. Skin-depth effects appeared negligible for frequencies below about 0.5 Hz, indicating that the magnetic field was permeating the whole volume of the toroid. Although the measurement was taken with the cores inserted in the gaps, the magnetic energy is dominated (again because of the much larger volume) by the yokes. The measured inductance, about 16 mH, agrees well with the predicted one of about 18 mH (assuming infinite permeability). The approximations used in estimating the inductance (gaps small compared to total toroid circumference, radial uniformity of the magnetic field) prevent us from extracting a more accurate value for the permeability. Our best estimate is that $\mu_{\mathrm{Toroid}} \approx 70$.

B. Systematic magnetic effects

In order to exploit the potential sensitivity of our spin source it is necessary to ensure that systematic magnetic effects are kept as small as possible. To estimate the relative importance of these effects we have assumed a torque reference level of 10^{-15} Nm, as this is consistent with the level of systematic effects that were observed in a recently published new limit on mass-spin coupling forces [6].

One of the main systematic background effects that could mimic a new spin-dependent force results from the possible magnetic interaction of the test masses with residual magnetic fields and field gradients. Clearly this will also depend on the magnetic properties of the test masses that are used with our spin source. Where appropriate, we will use the measured properties of our copper test masses in order to obtain specific torque values.

1. Interaction between test mass and residual magnetic fields

In general, a test mass can have a permanent magnetic moment $\vec{m}$ (for example due to ferromagnetic impurities) and also an induced one (due to its susceptibility, which in the case of pure copper is $\chi(\mathrm{SI}) \approx -8 \times 10^{-6}$). Similarly, at the location of the test masses, we need to consider a permanent magnetic field $\vec{B}_0$ (due to trapped flux that is frozen through pinning forces) and also a modulated component $\vec{B}_{\mathrm{mod}}$ (due to mobile trapped flux or direct flux leakage from the electromagnet).

Given these contributions, the magnetic interaction energy can be written as

$$\begin{aligned} U_{\mathrm{mag}} &= -\left\{\vec{m}(\phi) - \frac{\chi}{\mu_0} V(\vec{B}_0 + \vec{B}_{\mathrm{mod}})\right\} \cdot (\vec{B}_0 + \vec{B}_{\mathrm{mod}}) \\ &= -\vec{m}(\phi) \cdot (\vec{B}_0 + \vec{B}_{\mathrm{mod}}) + \frac{\chi}{\mu_0} V \vec{B}_0 \cdot \vec{B}_0 \\ &\quad + \frac{2\chi}{\mu_0} V \vec{B}_0 \cdot \vec{B}_{\mathrm{mod}} + \frac{\chi}{\mu_0} V \overrightarrow{B_0 + B_{\mathrm{mod}}}) \end{aligned} \tag{17}$$

where V is the volume of a test mass (in our case $V \approx 2 \times 10^{-7}\ \mathrm{m}^3$).

The variation of the components of the permanent magnetic moment of the test masses with angular motion, φ, can be characterized as

$$\begin{aligned} m_x &= m_{x0} \cos\phi - m_{y0} \sin\phi, \\ m_y &= m_{x0} \sin\phi + m_{y0} \cos\phi. \end{aligned} \tag{18}$$

The torque terms due to the permanent dipole moment can therefore be calculated as

$$\begin{aligned}\Gamma_z &= -\partial_\phi U_{\mathrm{mag}} \\ &= -\partial_\phi \vec{m} \cdot (\vec{B}_0 + \vec{B}_{\mathrm{mod}}) \\ &\quad - \vec{m} \cdot (x\partial_y - y\partial_x)(\vec{B}_0 + \vec{B}_{\mathrm{mod}}) \end{aligned} \tag{19}$$

where, to enable us to calculate the Cartesian derivatives of the fields, we have used the identity

$$\partial_\phi = x\partial_y - y\partial_x. \tag{20}$$

For the purposes of this discussion we can set $x = 0$ and y to be the radial distance of the test mass from the axis of rotation of the torsion balance which we have defined above to be R_{Tb}. The most problematic terms are obviously those modulated at the signal frequency. Considering only these terms we can find the modulated torque on the float as

$$\begin{aligned}\Gamma = R_{Tb}\Big\{ &\vec{m} \cdot \partial_x \vec{B}_{\mathrm{mod}} - \frac{2\chi}{\mu_0} V(\partial_x \vec{B}_0) \cdot \vec{B}_{\mathrm{mod}} \\ &- \frac{2\chi}{\mu_0} V \vec{B}_0 \cdot (\partial_x \vec{B}_{\mathrm{mod}}) \Big\} + \vec{m} \times \vec{B}_{\mathrm{mod}}. \end{aligned} \tag{21}$$

In order to eliminate the possibility of systematic effects at the level of our target sensitivity, we need to measure, or place upper limits on, their magnitude. We deal with the first term in Eq. (21) by measuring the components in the sensitive direction, m_x and $\partial_x B_{\mathrm{mod},x}$. We then assume that the values for the x-components of the dipole moment and field gradient represent upper limits for the other Cartesian components (m_y and $\partial_x B_{\mathrm{mod},y}$, m_z and $\partial_x B_{\mathrm{mod},z}$) which we have not measured. This will give a conservative limit as the x-component of field will, most likely, be the most significant. We then add all the components in quadrature (equivalent to multiplying by $\sqrt{3}$). The second term in Eq. (21) is estimated using plausibility arguments on the possible size of $\partial_x \vec{B}_0$ and the measured $B_{\mathrm{mod},x}$. Constraints on the third term in Eq. (21) are obtained by combining a measured upper limit on $\vec{B}_0$ with the modulated gradient. The final term can be written $m_{x0} B_{\mathrm{mod},y} - m_{y0} B_{\mathrm{mod},x}$ and we estimate an upper limit for its magnitude using statistical arguments as $\sqrt{2} m_x B_{\mathrm{mod},x}$. Again this should be a conservative estimate.

2. Measurement of $B_{\mathrm{mod},x}$ and $\partial_x B_{\mathrm{mod},x}$

In order to measure the modulated residual field and field gradient at the location of the test mass, we have carried out a dedicated series of experiments using a hand-wound superconducting gradiometer. The gradiometer is fabricated from lead (Pb) and coupled to a Quantum Design DC SQUID magnetometer. Imperfections in the manufacture of the gradiometer lead to a nonzero response even to uniform fields. This, in principle, undesired feature has been used to measure the uniform component as well. The response of the gradiometer to a known magnetic field and field gradient was first calibrated at room temperature using AC measurements, and then verified in a separate low-temperature experiment, where the predicted and measured responses agreed to within 10%. The gradiometer was then placed inside one of the cores, with the superconducting Nb tubes inserted, to measure the residual field and field gradients. In general, the voltage on the SQUID output at the modulation frequency will be the sum of three possible contributions: (i) the voltage due to residual flux leakage into the gradiometer circuit, (ii) the voltage due to a field gradient, and (iii) the voltage due to a uniform field. The different contributions can, in principle, be disentangled as follows. First, we have the option of keeping the gradiometer in place and simply swapping its electrical connections to the remainder of the circuit. The pickup voltage, by definition, is a result of flux coupling into other parts of the circuit. Reversal of the electrical connections will leave the pickup unchanged while reversing any signal from the gradiometer. Second, we can keep the electrical polarity the same, but physically turn the gradiometer by 180°. In this case only the response to a uniform field is reversed. Thus by making these measurements the three individual components can be estimated. We have carried out these measurements during successive cool-downs, using a current of 1 A through the spin source. Since the pickup voltage was by far the largest contribution, and it might have its origin (at least to some extent) in residual trapped flux, it is possible that these measurements do not show conclusively the presence of modulated magnetic fields and gradients. The amount of trapped flux can vary more or less randomly between separate cool-downs. In order to verify the reproducibility of the results, we warmed up the whole experiment to room temperature, cooled it down again and repeated the last measurement. We found a significant difference and it appears, therefore, that the real uncertainty of our measurements is significantly larger than the statistical one alone. As a result our quoted upper limits include such a systematic uncertainty. Solving for the field and field gradient terms we found $B_{\mathrm{mod},x} < 1.9 \times 10^{-10}$ T and $\partial_x B_{\mathrm{mod},x} < 1.7 \times 10^{-9}$ T/m, respectively.

3. Measurement of $\vec{B}_0$ and estimate of $\partial_x \vec{B}_0$

We have searched for a DC magnetic field inside the niobium superconducting tubes in a separate experiment using the Hall probe, but have not found any nonzero field. The experimental resolution allows us to place an upper limit of $|\vec{B}_0| < 2 \times 10^{-5}$ T. We have not attempted to measure the residual DC magnetic field gradient at the location of the test masses. However, it seems plausible that the gradient cannot be much larger than the DC field itself, divided by the size of the interaction region. With an inner diameter of the niobium tubes of 7 mm, we obtain $|\partial_x \vec{B}_0| \leq 2.9 \times 10^{-3}$ T/m.

4. Limits on systematic background effects

Given the numbers above, we can now analyze the four torque terms in Eq. (21) to see if they are significant in comparison with the target sensitivity of 10^{-15} Nm. In order to estimate the first term, we have carried out a dedicated experiment to measure the permanent dipole moment of one of our test masses. We have removed the magnetic shielding, and deliberately exposed one test mass to a known magnetic field and field gradient. We found no significant torque at the modulation frequency, and this allows us to set a limit of $m_x \leq 7.5 \times 10^{-10}$ Am^2. Table II shows the contributions of the four magnetic effects to the total torque, taking into account that limits on only one vector component have been measured. We have accounted for the presence of three test masses by multiplying by a further factor of $\sqrt{3}$.

With a combined systematic uncertainty of around 4×10^{-19} Nm, these torques are well below the target sensitivity of 10^{-15} Nm. It is worth noting that we have only established upper limits on these residual magnetic couplings. Magnetic fields or field gradients were not conclusively found at the location of the test masses. More sensitive measurements might be used to constrain systematic background effects further.

5. Direct Magnetic Pickup

There is also the possibility of direct magnetic pickup between the spin-source drive current and the SQUID pickup loop. This source of uncertainty was addressed in two ways. First, two pairs of wires were incorporated into the superconducting Pb tube which took the spin-source charging wires into the vacuum can. The first pair of wires were used to energize the spin source while the second set of wires (or dummy charging wires) were simply terminated at the toroid. In this way any magnetic pickup between the charging wires and the SQUID pickup loop could be estimated. No significant signal was measured during the experimental runs. Furthermore, a pickup measurement was performed before every experimental run with the torsion balance float sitting down on the levitation bearing. In this case any measured signal on the SQUID must have been due to induced pickup and could be subtracted from the data set taken when the float was levitated.

TABLE II. Limits on the magnitude of the residual magnetic interactions.

Magnetic interaction term	Torque magnitude [Nm]
$R_{Tb}(\vec{m} \cdot \partial_x \vec{B}_{\mathrm{mod}})$	1.6×10^{-19}
$R_{Tb} \frac{2\chi}{\mu_0} V \partial_x \vec{B}_0 \cdot \vec{B}_{\mathrm{mod}}$	1.8×10^{-19}
$R_{Tb} \frac{2\chi}{\mu_0} V \vec{B}_0 \cdot \partial_x \vec{B}_{\mathrm{mod}}$	1.1×10^{-20}
$\vec{m} \times \vec{B}_{\mathrm{mod}}$	3.5×10^{-19}
Total (quadrature sum)	4.2×10^{-19}

A small pickup, which remained fairly constant during the experimental runs, was measured and we believe this originated from trapped magnetic flux moving around in the Pb shields (described in more detail in Ref. [6]).

C. Systematic thermal effects

When the spin source is magnetized we can expect dissipative mechanisms to result in heating of the toroid. At low temperatures, where the specific heat of materials is low, the deposited heat can lead to significant temperature changes in the spin source and torsion balance. Furthermore, the temperature variation produces thermal torques on the output of the torsion balance which we believe are due to changes in the configuration of trapped flux coupling the float to the bearing. We have identified three possible sources of heat dissipation in the spin source, and we will address them in the following sections. It should be noted that a full understanding of the heating mechanism requires further investigation and that the following sections present some qualitative estimations of the effects. We believe that this approach is justified because although heating can produce torques at the signal frequency we were able to eliminate them as the main source of error in the experiment. This was achieved by purposely inducing a large and easily measured effect which could be extrapolated to reduce the thermal torques to 1 order of magnitude below the reference level (10^{-15} Nm). Therefore it is the origin of the systematic thermal effects that we address with these qualitative arguments.

1. Thermal model of the spin source

In order to convert the temperature rise observed during the magnetization of the spin source into a dissipated power we need to know the specific heat of the toroid and its thermal resistance to the surroundings at 4.2 K. A convenient method for finding this is to apply a known power to the spin source and measure the resulting temperature increase. This was performed in a dedicated experiment that incorporated a heater wire wrapped around the spin source and an Allen-Bradley resistance thermometer located within a hole drilled in the soft-iron toroid. Both the heater and the thermometer were thermally coupled to the spin source with Apiezon N grease. By inputting a square wave current into the heater the subsequent temperature rise and thermal time constant for cooling were measured. A continuous input power of 200 μW resulted in a temperature rise of 0.2 mK. It is believed that the main heat loss mechanism for the spin source is through the residual helium exchange gas in the vacuum can. This is the role of the gas and results in a measured thermal time constant of 26 s. When the residual helium gas was removed with a charcoal getter the time constant was in excess of 200 s. This supports the conclusion that the exchange gas is the primary heat dissipation mechanism. It should be noted that it is possible that the experiment

may overestimate the power required to induce a given temperature change. This is a common problem in low-temperature calorimetry where it can be difficult to ensure that all of the input power is effectively coupled into the sample under test. Furthermore, the heating effects observed during magnetization of the spin source are AC effects while the calibration was performed at DC. We have scaled the calibrated power appropriately to account for this difference.

2. Measured heating in the toroid

Potentially problematic is the fact that heating can induce signals that can occur at the drive frequency of the spin source. Figure 9(a) shows a plot of the temperature change of the toroid when a sinusoidal current modulation at 10 mHz and amplitude 1 A is applied. For this measurement an offset of 0.1 A was purposely induced on the drive current and this also resulted in an offset in the H-field. The maximum temperature change is approximately 0.2 mK and the dominant heating occurs at twice the signal frequency (20 mHz). Figure 9(b) shows the temperature spectral density of the time series which clearly indicates the 2ω component together with the fundamental frequency and higher harmonics. We have confirmed, during our experimental campaign [6], that an offset in the spin-source current can generate torques which have a coherent component at the modulation frequency. We were able to place limits on these systematic thermal torques by measuring their magnitude when offsets were purposely induced on the driving current. Figure 10 shows the measured in-phase and quadrature torques at the signal frequency as a function of the offset current on the spin-source modulation. The dominant heating effect is obtained in the quadrature channel although there is also a significant effect in the signal (in-phase) channel. This is fully consistent with a model that assumes that the thermal time constant for cooling is significant with respect to the modulation period of the spin source. We were able to reduce the thermal torques to $<10^{-16}$ Nm (an order of magnitude lower than the reference level) at the signal modulation frequency by ensuring that the offset current in the spin source was $<0.1\%$ of the drive amplitude for all our experiments.

In conclusion we find driving the spin source at a frequency of 10 mHz and amplitude of 1 A results in temperature rise in the toroid of approximately 0.2 mK (at 20 mHz). From the characterization measurements above we can estimate that a sinusoidal peak power of 280 μW is required to produce the measured temperature rise. Although we have shown that torques at the signal frequency can be minimized by ensuring the H-field contains zero offset, torques at twice the signal frequency cannot be minimized in this way. In the following sections we attempt to estimate the potential sources of heating that could give rise to the observed effects.

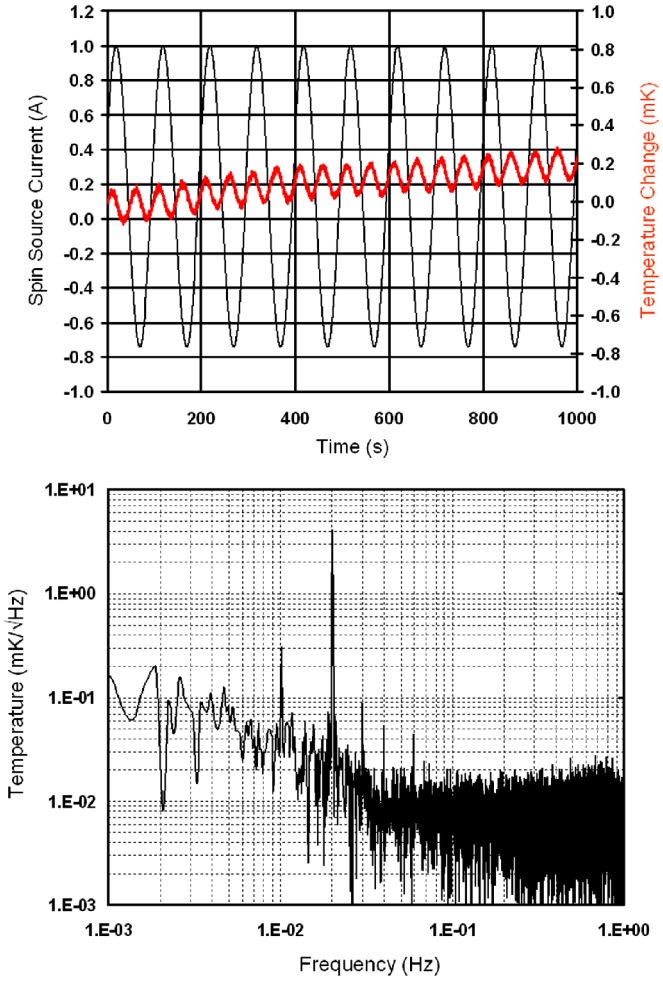

FIG. 9 (color online). (a). Temperature change in the toroid when a sinusoidal current modulation is applied. (b) Amplitude spectral density of the temperature variation.

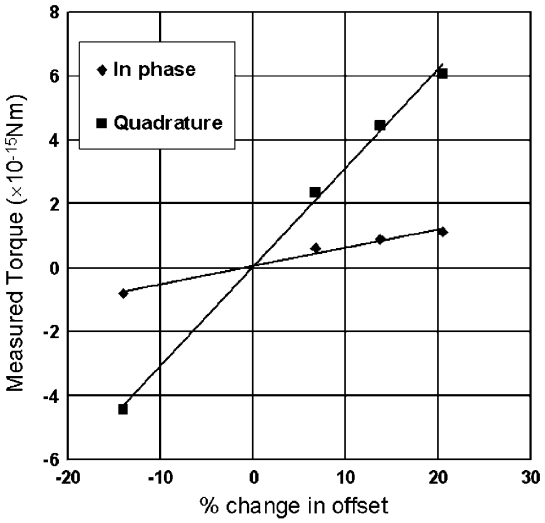

FIG. 10. In-phase and quadrature torques obtained when purposely applying an offset onto the spin-source drive current.

3. Heating due to hysteresis and the magneto-caloric effect

It was mentioned in Sec. IV A that hysteresis is observed between the driving current in the solenoid (or the H-field) and the magnetic field measured by the Hall probe. Hysteresis is a nonreversible process and results in a dissipated power when the system is cyclically taken around the hysteresis loop [18]. The net power loss, per unit volume, of the spin-source assembly has been estimated using Rayleigh's law [19,20]. In this formulation it is assumed that the magnetization of a sample, starting from the demagnetized state, varies quadratically with the applied H-field

$$M = aH_a + bH_a^2 \tag{22}$$

where the constants a and b are properties of the ferromagnetic material and H_a is the amplitude of the applied H-field. By oscillating the H-field between the peak values $\pm H_{\max}$ the system follows a closed hysteresis loop whose magnetization branches may be represented by parabolic curves

$$M \pm M_{\max} = a(H_a \pm H_{\max}) + b(H_a \pm H_{\max})^2 \tag{23}$$

where the plus and minus correspond to the ascending and descending cycles, respectively. The loop area, and therefore power loss per unit volume at frequency f, can finally be calculated as

$$\dot{Q}_{\text{hysteresis}} = \frac{4}{3}\mu_0 b f H_{\max}^3 = \frac{8}{3} f B_r H_m \tag{24}$$

with the remnant field $B_r = \frac{\mu_0 b}{2} H_m^2$. Assuming that the H-field varies as $H = H_a \cos\omega t$ we may write the magnetic field for the ascending/descending branches of the hysteresis loop as [21]

$$B = B_m \cos\omega t \pm B_r \sin^2\omega t. \tag{25}$$

Expansion of the $\sin^2\omega t$ to first order yields

$$B = B_m \cos\omega t + B_r\left(\frac{8}{3\pi}\sin\omega t + \ldots\right), \tag{26}$$

and the instantaneous power dissipation in the material, $\dot{Q}_{\text{inst}} = H\frac{dB}{dt}$, is

$$\dot{Q}_{\text{inst}} = \frac{1}{2}\omega H_m B_m \sin 2\omega t + \frac{8}{6\pi}\omega H_m B_r(1 + \cos 2\omega t). \tag{27}$$

It is interesting to note that the first term is equivalent to the energy stored in the magnetic field which averages to zero over a single cycle. The second term, which results from the phase difference between the H-field and the magnetic field, is a lossy component and results in energy deposition within the material. The power loss over an entire cycle is $8fB_rH_m/3$ which is identical to the expression in Eq. (24). Applying Rayleigh's law to our measured hysteresis curve (Fig. 8(a)) yields a net power loss of 10 μW per cycle. When combined with the thermal model of the spin source this gives a temperature rise of approximately 10 μK per cycle. This appears too small to explain the temperature variation shown in Fig. 9(a). It should be noted that this is probably only an estimate of the hysteretic loss in the spin source. Some authors have noted that at low levels of H-field [22] the quadratic variation assumed by Rayleigh's law is not observed, and that a linear relationship is more appropriate.

A second heating mechanism related to magnetization is the magneto-caloric effect. It is well noted in the literature [23] that magnetizing/demagnetizing a sample can result in a heating/cooling. The basic mechanism is that magnetizing the system reduces the magnetic entropy through ordering of the material. In order to conserve the total entropy of the system the component due to the thermal energy, and therefore temperature of the sample, increases. When demagnetizing the sample, the magnetic entropy increases and this corresponds to a reduction in temperature. The process is reversible and would result in a temperature variation at twice the modulation frequency. If hysteresis is neglected, equilibrium thermodynamics results in the following Maxwell relation between the magnetization and the entropy [23]:

$$\mu_0\left(\frac{\partial M}{\partial H}\right)_T = \left(\frac{\partial S}{\partial H}\right)_T, \tag{28}$$

which is an equivalence between the rate at which the magnetization changes at constant temperature and the rate at which the entropy changes at constant temperature. However, this relationship cannot be used when a sample exhibits hysteresis as the system is out-of-equilibrium and dissipative processes produce an additional entropy change. To describe the temperature changes along the hysteresis loop requires consideration of the system degrees of freedom which are coupled to the applied H-field (the magnetic subsytem) and the remaining degrees of freedom not coupled to the H-field (the nonmagnetic subsytem) [23]. In Ref. [23]., the authors deal with iron at room temperature and use the assumption that the specific heat capacity is large in order to calculate the entropy associated with the two processes. However, at low temperature, it is not clear whether this assumption is still valid. As a result we have not yet calculated the heating due to the magneto-caloric effect and can only say that such a mechanism could certainly give rise to temperature rises at twice the modulation frequency.

4. Heating due to eddy currents

The applied H-field will induce eddy currents in the core of the toroid which can lead to dissipation through the resistance of the soft-iron. The currents will flow in a skin depth, δ, which is given by

$$\delta = \sqrt{\frac{\rho}{\mu_0 \mu \pi f}} \tag{29}$$

where ρ is the resistivity and μ is the relative permeability of the toroid material. If we assume that the resistivity of the iron toroid reduces by a factor of approximately 100 from its room temperature value [24] and that the spin source is modulated at 12.5 mHz we find that the skin depth is approximately 20 mm. This is consistent with our measurements in Sec. IV A that suggested that the magnetic field permeates the entire volume of the spin source. The power loss per cycle can be estimated from the following analytical expression for a cylindrical body of length L [20]:

$$\dot{Q}_{\text{eddy}} = \frac{\pi R^4 L \omega^2 B_0^2}{16\rho}, \tag{30}$$

where B_o is the peak applied magnetic field and R is the mean radius of the toroid. Using the spin-source dimensions quoted in Table I and a peak magnetic field of 2.2×10^{-2} T we can estimate the power loss per cycle as 170 μW. Furthermore this heating effect will appear at twice the modulation frequency as it is proportional to the square of the magnetic field. It appears plausible that the observed 2ω temperature signal could be due to eddy current losses in the toroid. A power loss of 170 μW would result in a temperature rise of approximately 0.12 mK which is certainly consistent with the measured effect shown in Fig. 9(a).

V. SUMMARY AND CONCLUSIONS

We have designed, constructed, and characterized a novel spin source that is currently being used to search for new short-range interactions coupling to quantum mechanical spin. The polarization of the spins in our source is modulated using an external current. A unique feature of our design is that the magnetic field associated with the spins is actually *used* to cancel the magnetic field that polarizes them. The measurement is made in an environment where there can be, in principle, no background magnetic field. The spin source is operated in a cryogenic environment, which enables us to further suppress any residual magnetic field using highly effective superconducting shields.

We find that our source exhibits a spin density comparable with that of other spin sources used in previous experiments. One feature that is unique to our spin source is that the orientation of the aligned spins can be reversed electronically, rather than mechanically.

Combined with a torque sensitivity of approximately 10^{-15} Nm, our spin source has been used to improve existing constraints on scalar-pseudoscalar coupling constants by about 10 orders of magnitude at a range of 1 mm [6]. We have shown that systematic torques due to magnetic impurities are insignificant ($< 10^{-19}$ Nm) and that thermal torques can be controlled at the level of $<10^{-16}$ Nm by ensuring that the driving current is symmetric. We are currently modifying our experiment in order that the spin source can be located in the helium bath to remove heating effects and simplify magnetic shielding.

ACKNOWLEDGMENTS

We would like to thank Dr T. J. Quinn, FRS of the Institute of Physics (UK) and Royal Society Paul Fund, the Leverhulme Foundation and STFC (formerly PPARC) for financial support for this work. We would also like to thank the mechanical workshops at the University of Birmingham and Imperial College, London, for fabricating the experimental components described in this work.

[1] J. Leitner and S. Okubo, Phys. Rev. B **136**, B1542 (1964).
[2] R. Peccei and H. Quinn, Phys. Rev. Lett. **38**, 1440 (1977).
[3] C. T. Hill and G. G. Ross, Nucl. Phys. **B311**, 253 (1988).
[4] P. Fayet, Classical Quantum Gravity **13**, A19 (1996).
[5] J. E. Moody and F. Wilczek, Phys. Rev. D **30**, 130 (1984).
[6] G. D. Hammond, C. C. Speake, C. Trenkel, and A. Pulido Patón, Phys. Rev. Lett. **98**, 081101 (2007).
[7] W-T. Ni, S-S. Pan, H-C. Yeh, L-S. Hou, and J. Wan, Phys. Rev. Lett. **82**, 2439 (1999).
[8] A. N. Youdin, D. Krause, Jr., K. Jagannathan, and L. R. Hunter, Phys. Rev. Lett. **77**, 2170 (1996).
[9] T-H. Jen, W-T. Ni, S-S. Pan, and S-L. Wang, in *Proceedings of the 6th Marcel Grossmann Meeting on General Relativity*, edited by H. Sato and T. Nakamura (World Scientific, Singapore, 1992), p. 489.
[10] A. Pulido-Patón, Ph.D. thesis, University of Birmingham, 2004.
[11] G. D. Hammond, A. Pulido-Paton, C. C. Speake, and C. Trenkel, Rev. Sci. Instrum. **75**, 955 (2004).
[12] D. Shaul, T. J. Sumner, G. K. Rochester, and C. C. Speake, Classical Quantum Gravity **13**, A107 (1996).
[13] C. Trenkel, Ph.D. thesis, University of Birmingham, 1997.
[14] C. Trenkel and C. C. Speake, Supercond. Sci. Technol. **14**, 190 (2001).
[15] R. C. Ritter, L. I. Winkler, and G. T. Gillies, Phys. Rev. Lett. **70**, 701 (1993).
[16] M. G. Harris, Ph.D. thesis, University of Washington, 1998.
[17] B. R. Heckel, University of Washington (unpublished).
[18] F. Bitter, Phys. Rev. **38**, 528 (1931).
[19] L. Rayleigh, Philos. Mag. **23**, 225 (1887).
[20] G. Bertotti, *Hysteresis in Magnetism* (Academic Press,

New York, 1998), p. 310.
[21] R. Bozorth, *Ferromagnetism* (Van Nostrand, Macmillan Publishing, New York 1951), p. 778.
[22] J. A. Baldwin, Jr., J. Revol, and F. Milstein, Phys. Rev. B **15**, 426 (1977).
[23] V. Basso, M. Bertotti, M. LoBue, and C. P. Sasso, J. Magn. Magn. Mater. **654**, 290 (2005).
[24] http://hypertextbook.com/facts/2004/JonathanRuditser.shtml.